Smart Structures and Systems, *Vol. 27, No. 2 (2021) 387-396*
DOI: https://doi.org/10.12989/sss.2021.27.2.387

Addition of passive-carriage for increasing workspace of cable robots: automated inspection of surfaces of civil infrastructures

Guillermo Rubio-Gómez [1], Sergio Juárez [1], David Rodríguez-Rosa [1], Enrique Bravo [1], Erika Ottaviano [2], Antonio Gonzalez-Rodriguez [1] and Fernando J. Castillo-Garcia*[1]

[1] *School of Industrial and Aerospace Engineering, Av. Carlos III, 45071 Toledo, Spain*
[2] *DICeM, University of Cassino and Southern Lazio, Via G. Di Biasio 43, 03043 Cassino, Italy*

(*Received July 16, 2020, Revised September 28, 2020, Accepted October 10, 2020*)

Abstract. Cable-driven robots are parallel manipulators in which rigid links are replaced by actuated cables. The end-effector is then supported by a set of cables commanded by motors that are usually placed in a fixed frame. By varying the cables length, it is possible to change the end-effector position and/or orientation. Among the advantages presented by cable robots are they light-weight structure, high energy efficiency and their ability to cover large workspaces since cables are easy to wind. When high-speed operation is not required, a safer solution is to design cable-driven suspended robots, where all vertical components of cables tension are against gravity direction. Cable-driven suspended robots present limited workspace due to the elevated torque requirements for the higher part of the workspace. In this paper, the addition of a passive carriage in the top of the frame is proposed, allowing to achieve a much greater feasible workspace than the conventional one, i.e., with the same size as the desired inspection area while maintaining the same motor requirements. In the opposite, this new scheme presents non-desired vibration during the end-effector maneuvers. These vibrations can be removed by means of a more complex control strategy. Kinematics and dynamics models are developed in this paper. An analysis of sensor system is carried out and a control scheme is proposed for controlling the end-effector pose. Simulation and experimental results show that the feasible workspace can be notoriously increased while end-effector pose is controlled. This new architecture of cable-driven robot can be easily applied for automated inspection and monitoring of very large vertical surfaces of civil infrastructures, such as facades or dams.

Keywords: parallel robot; cable-driven robot; dynamics model; vibration control; automated inspection

1. Introduction

Inspection and maintenance of steel and composite large vertical structures are critical issues for sustainability of existing and new infrastructures (Huang *et al*. 2016). Classical approaches rely on large human activities eventually performed in unsafe conditions (Lee *et al*. 2010). Overcome the problem using robots, UAV or on site contactless global automated measurements for self-inspection and maintenance can be pursued at the present state-of-art of the current mechatronics (Jung *et al*. 2019, Kim *et al*. 2014).

Cable-Driven Parallel Manipulators (CDPMs) are a class of parallel robots in which, instead of using rigid bodies only, the fixed frame and platform are connected by several cables, which can be exerted or retracted by an actuation systems. Cables are wounded around drums that are fixed on the frame and suitable actuation and transmission system composed by rotary motors and pulleys allow controlling the length and direction of the cables to operate a tool, called end-effector. Main characteristics are a very large workspace, lightweight structure and relatively low-cost systems. In particular, the reduction of the moving masses may lead to good dynamic properties; in addition, changing the configuration for the actuation and pulleys the CDPM can be reconfigured, being also modular. These are important features for applications requiring a manipulator being brought to work on site.

CDPM were introduced a few decades ago, but they have become much more interesting from theoretical and applied research than their classical counterparts composed by rigid links only. More specifically, if classical parallel manipulators are still used and mainly confined as motion simulators, CDPM ranges from industry, entertainment, rehabilitation and recently civil engineering, just to cite some.

One of the first application of cable systems is RoboCrane (Bostelman *et al*. 1996). It uses the basic idea of the Stewart platform parallel manipulator but adding cables. The NIST RoboCrane has the capacity to lift and precisely manipulate heavy loads over large volumes with fine control in all six degrees of freedom. In addition, NIST developed an advanced RoboCrane controller. The graphic off-line control capability of this controller made programming of numerous controllers easy and fast (Bostelman *et al*. 1996).

Kawamura presented in Kawamura *et al*. (1995) an ultrahigh speed robot design, FALCON-7 that is a cable-driven parallel system. The introduction of elasticity in the

*Corresponding author, Professor,
E-mail: fernando.castillo@uclm.es

http://www.techno-press.org/?journal=sss&subpage=7
ISSN: 1738-1584 (Print), 1738-1991 (Online)

cables modelled as nonlinear spring improved the system transient response, but it also complicated the study of stability. Their experimental results showed stable manipulator performance. Further development of the model was proposed in Kawamura *et al*. (2000) to reduce vibration.

A large CDPM was developed to be applied as advanced virtual reality simulator (CableRobot Simulator 2020), in which the motion of the cabin is controlled by eight unsupported steel cables attached to winches. A CDPM was proposed in Yangwen *et al*. (2010) as suspension system for airplane model testing in low-speed wind tunnel, also proposing a method for measuring the aerodynamic parameters of the airplane model.

Very large CDPM developed for load transportation in industrial environment are manipulators belonging to the IPAnema family of CDPM, described in Pott *et al*. (2013); CoGiRo project 2020) The Five hundred meter Aperture Spherical Telescope (FAST) was originally described in (Nan 2006). The above-mentioned CDPM act in a crane configuration. Such robots, also called as Cable-suspended robots, are very well suited for suspended camera systems that are widely used in stadiums and arenas. Such systems consist of three major components: the reel—the motor drive and cables, the spar—the counterbalanced pan and tilt video camera, and central control, the computer software used by the operator to fly the camera (Cone 1985, Skycam 2020).

A limitation on the use of CDPMs are related to the mechanical feature of the cables, which can only work in tension. Therefore, the pose is feasible only for cables' configuration in which the static or dynamic equilibrium is assured under the constraint that the internal cable axial force must be positive. Although first research on the subject have treated cables as inextensible and massless, assuming them as perfect lines connecting the end-effector and pulleys (Roberts *et al*. 1998) it has been shown that axial and transversal flexibility should be considered for correct modelling. In particular, the axial flexibility can be taken into account as an equivalent stiffness model as it was proposed in Behzadipour (2006) for a single cable with pretension, using four springs. Lately, the current approach is to introduce mass of the cables taking into account transversal flexibility, either considering lumped masses (Ottaviano and Castelli 2010, Castelli *et al*. 2014) or continuum mass modeling (Merlet and dit Sandretto 2015, Ottaviano *et al*. 2019).

An interesting class of CDPMs is that in a crane configuration (also called suspended CDPM), in which gravity acts like an additional cable, and not all the end-effector DOFs can be controlled. Crane-type CDPM have attracted the interest of theoretical and applied research because they offer several advantages, such as the reduction of the number of cables, the overall costs and setup time, improved ease of assembly and a lower possibility of cable interference.

Referring to the kinematic study of suspended CDPMs, the challenging problem is that less than 6 DOFS may be controlled, so that when the cable lengths are assigned the end effector still has some freedom. Thus, its actual pose is determined by the wrenches acting upon it Abbasnejad and Carricato (2015) in which the problem has been defined as geometrico-static also expressing some connections between stability and energy.

The suspended CDPM presents limited workspace due to both tension limitations in real applications, i.e., upper bounds due to motor power and lower bounds due to low tensions at the lateral boundaries of the workspace yielding to worst end-effector positioning capabilities. Pulleys greatly influence the position capabilities of suspended CDPM, as it was shown in (Gonzalez-Rodriguez *et al.* 2017).

A passive carriage can be designed and added at the top of the frame, as it is proposed in this paper, achieving a larger workspace than the suspended CDPM one, i.e., with the same size as the desired inspection area. In the opposite, this new scheme presents non-desired vibration during the end-effector maneuvers. These vibrations can be removed by means of a more complex control strategy. The proposal is easily scalable and can be applied for inspection of large vertical surface of civil structures.

This paper is structured as follows: Section 2 describes the basics of suspended cable robots and the new proposal for increasing its workspace. Section 3 presents the kinematic and dynamics models for the proposed robot. Section 4 explains the control strategy developed for the proposed robot. Section 5 present the modelling and simulation results, showing that the workspace is increased without losing the end-effector controllability. Section 6 shows the experimental facility developed for the validation of the robot and the results obtained. Finally, section 7 states the main conclusions and further works.

(a) Commanded configuration (b) Suspended configuration

Fig. 1 Example of Commanded and Suspended configurations of CDPM

2. New proposal description

2.1 Basics

As aforementioned Cable-Driven Parallel Manipulators can be classified in Suspended or Commanded when all the vertical components of cable tension are against gravity direction or not, respectively (Pusey *et al*. 2004). For illustrative purpose, Fig. 1 represents a suspended and commanded configuration of a planar cable-driven robot in a vertical plane. In both schemes, the end-effector, which carries the inspection device that can be a camera (Adhikari *et al*. 2014) or laser (Wang *et al*. 2016), the frame and the cables are represented.

Commanded configuration requires a perfect synchronous control of cables' length but allows to move the end-effector with greater acceleration than 1G in the gravity direction by Gouttefarde (2008). On the contrary, suspended configuration is mechanically safer because a non-synchronous control of cables' length does not yield to destructive scenarios, but it only can move the end-effector at 1G in the gravity direction (Roberts *et al*. 1998). This work proposes a planar CDPM for large vertical surface inspection tasks.

Following sections describes the workspace limitation of conventional Cable-Driven Suspended Robot (CDPM) and the new proposal to obtain a feasible solution for a complete workspace inspection.

2.2 Workspace limitation

Workspace limitation of CDPM are related to the actuator system and the cables. End-effector pose is controlled by cable length variations. Cable lengths are typically controlled by means of the actuator system: a motor (usually coupled to a gearbox) and a winch. This winch angle is controlled by the motor and cable rolls in or out on it. As consequence, by controlling motor angles, cable length can be controlled, and the end-effector can be therefore positioned at the desired pose.

When the end-effector is placed at the upper part of the workspace, cables' tension is too high, due to the greater angle between cables and the vertical. This yields the need in motors to exert a very high torque to maintain the end-effector pose or to modify it (Rubio-Gómez *et al*. 2019). In this sense, the upper part of the workspace is inaccessible owing to the natural torque limitation of the motors (see Fig. 2, region A). On the other hand, when effector is located at the lateral areas of the workspace, some of the cable tensions are to low and cables suffer saggy effect Arsenault (2013) and the end-effector desired pose is lost (see Fig. 2, region B).

The size of the regions A and B with regards to the frame size depends of the frame width and height, the end-effector width and height, the mass of the end-effector and the cables. More details of this workspace limitation can be found in Fattah (Fattah and Agrawal 2002) or Castelli (Castelli *et al*. 2010).

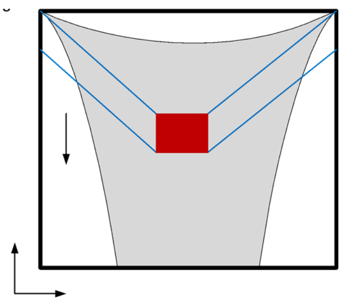

Fig. 2 Workspace limitation of conventional CDPM

2.3 New proposal

Our proposal is focused on enlarging the workspace of CDPMs without increasing the number of actuators. Adding a passive carriage (without active actuation) in the top of the frame and connecting the end-effector to the actuated winch though this passive carriage the workspace can be notoriously increased. Fig. 3 shows the new proposal together with the analogous conventional CDPMs for the planar case.

A simple analysis based on the static equilibrium of end-effector and carriage yields that, for the same active node, i.e., same motor-winch set, and the same cables, the workspace is notoriously increased. On the contrary, for the same end-effector position, our proposal presents an important drawback: the rigidity of the system decreases and the end-effector presents non-desirable vibrations (similar to a pendulum) which need to be controlled. Simulation Section details the workspace analysis together with the frequency characterization of the system.

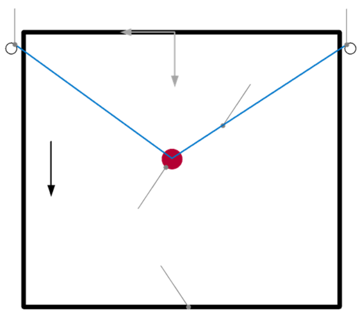

(a) Conventional configuration

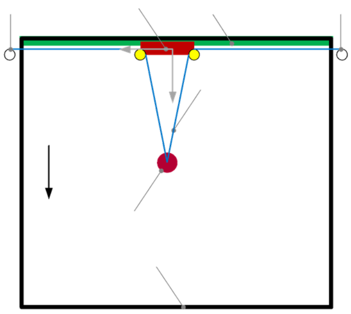

(b) New proposal

Fig. 3 Planar CDPMs

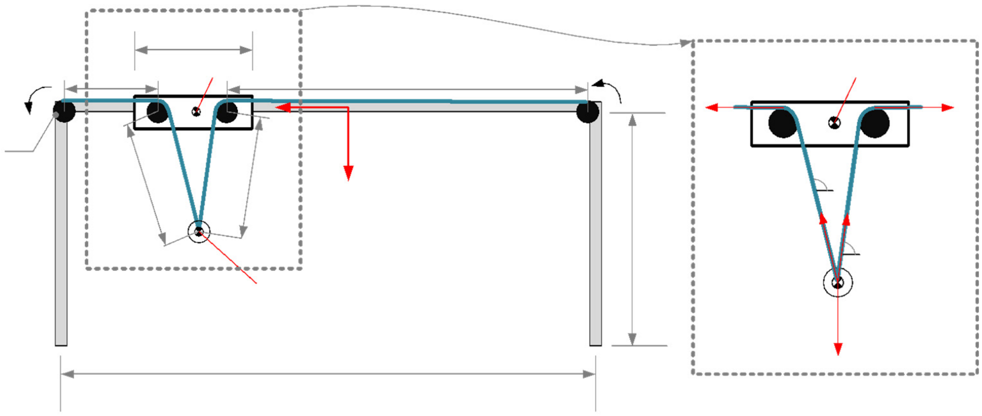

Fig. 4 Nomenclature for mathematical model

3. Mathematical model

3.1 Nomenclature

Fig. 4 represents the robot scheme including the nomenclature that is used for the mathematical formulation.

The dimensions of the frame are $W \times H$. The width of the carriage is w and its mass is m_c. The cable lengths are L_1, L_2, L_3 and L_4 according to the Scheme in Fig. 4 and the angles of segments L_2 and L_3 are α_L and α_R, respectively. The radius of the winches (active nodes) is r, since their angular position are θ_L and θ_R, respectively. The end-effector mass is m_e and its position is $[x_e, y_e]^T$. Finally, the tension of the cable of the left and the right segments are T_L and T_R, respectively.

3.2 Kinematic analysis

The system described in the proposal has three Degrees-Of-Freedom (DOF), x_e, y_e and x_c but only two controllable inputs, θ_L and θ_R. In this sense, for a given pair of value motor/winch angles, θ_L and θ_R, multiple combination of x_e, y_e and x_c can be found. Inverse kinematic problem consists on determining the required motor/winch angles, θ_L and θ_R, for positioning the end-effector in the desired position. On the contrary, the forward kinematic problem consists on determining where is the end-effector placed for a given pair of motor angle values, θ_L and θ_R. The inverse kinematic problem can be therefore expressed as $[\theta_L, \theta_R] = \Lambda^I(x_e, y_e, x_c)$ an has a unique solution. The forward kinematic problem has been denoted as $[x_e, y_e, x_c] = \Lambda^F(\theta_L, \theta_R)$ and has infinity solutions (Pott 2018a). The inverse kinematics will be applied to develop the dynamics model and in the control scheme for controlling the end-effector pose. The expression of Λ^I is detailed in Appendix A.

3.3 Dynamics model

This model describes the dynamic behavior of the system. The input variables are the torque exerted by the motors, τ_L and τ_R, and the output is the end-effector position, x_e and y_e (see Fig. 5).

Fig. 5 Dynamic model of the system

Under the assumption of non-extensible cables (Pott 2018b) the dynamics of the motor/winch sets, end-effector and carriage must be considered to develop a simple but representative model

$$
\begin{aligned}
m_e \ddot{x}_e &= T_L\, cos\, \cos(\alpha_L) + T_R\, cos\, \cos(\alpha_R) \\
m_e \ddot{y}_e &= m_e g - T_L\, sin\, \sin(\alpha_L) - T_R\, sin\, \sin(\alpha_R) \\
m_c \ddot{x}_c + b_c \dot{x}_c &= T_L(1 + cos\, cos\, (\alpha_L)) \\
&\quad - T_R(1 - cos\, cos\, (\alpha_R)) \\
\tau_L &= J_L \ddot{\theta}_L + b_L \dot{\theta}_L + T_L r \\
\tau_R &= J_R \ddot{\theta}_R + b_R \dot{\theta}_R + T_R r
\end{aligned}
\tag{1}
$$

being b_c the viscous friction coefficient of the carriage/linear guide, J_L and J_R the moments of inertia of the left and right motor/winch sets and b_L and b_R the viscous friction coefficient of the left and right motor/winch sets.

4. Control strategy

Let's denote $[x_e^*, y_e^*]$ the desired end-effector pose, and let's also assume that in steady state $x_e = x_c$. Under the point of view of the control two overall alternative are possible: (a) to directly control the end-effector position $[x_e, y_e]$ by measuring and feeding back it (control in *objective coordinates*); (b) to indirectly control the end-effector position by using inverse kinematics and measuring and feeding back the motor/winch coordinates (control in *joint coordinates*). Both strategies are shown in Fig. 6.

Control in *objective coordinates* requires an accurate and fast enough measurement of end-effector position (for example vision system). In addition, the controller dimension is 2×2 and 4 controllers block should be tuned. On the other hand, control in *joint coordinates* is more frequently applied because only require joint coordinates measurement (for example encoders) and only

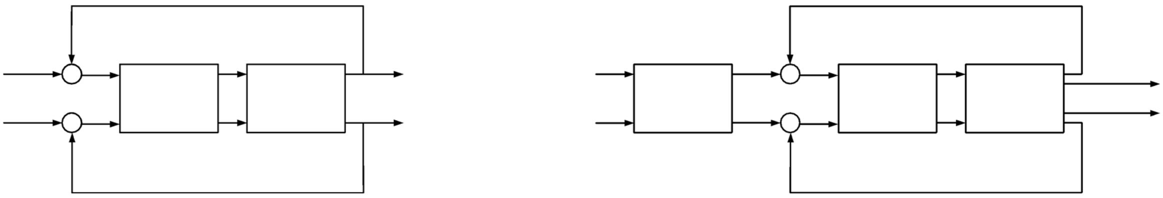

(a) Control in objective coordinates (b) Control in joint coordinates

Fig. 6 Feasible control strategies

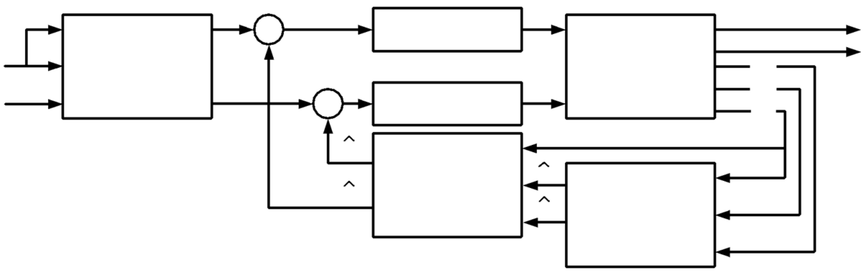

Fig. 7 Control scheme for positioning end-effector

two 1×1 uncoupled controllers must be tuned (Castillo-Garcia *et al.* 2017). Our control strategy is therefore based on control in joint coordinates but control scheme of Fig. 6(b) cannot be directly applied owing to the multiple solution of forward kinematics. In this sense, control scheme at Fig. 6(b) must be modified to obtain a unique solution of $[x_e, y_e]$ by measuring the joint coordinates, θ_L and θ_R together with the carriage position, x_c. The final control scheme is presented in Fig. 7. Note that an estimator block has been added in order to estimate the end-effector pose, $\hat{x}_e$ and $\hat{y}_e$, by means of the measurement of carriage position and motor/winch sets angular position, $[\hat{x}_e, \hat{y}_e] = \Xi(x_c,\ \theta_L, \theta_R)$. The expression of the estimator is detailed in Appendix A. In addition, a reference value of carriage position has been also added assuming steady state conditions ($x_e^* = x_c^*$).

Following sections show that both, simulations, and experimental results demonstrate the ability of this control scheme for controlling the end-effector pose. PID controllers have been tuned as controller block for demonstrating the feasibility of our robot proposal but other control techniques can be easily applied. Dynamics model (1) is nonlinear. In this way, controller blocks shown in Fig. 7 should be non-linear or linear but robust enough to compensate the non-linear behavior of the system. As control is defined in joint coordinates, dynamics of actuator can be rewritten as

$$\begin{aligned} \tau_L &= J_L \ddot{\theta}_L + b_L \dot{\theta}_L + z_L \\ \tau_R &= J_R \ddot{\theta}_R + b_R \dot{\theta}_R + z_R \end{aligned} \tag{2}$$

being z_L and z_R disturbances that the motors suffer which actually model the payload variation of the motors owing to the cables tension. Therefore, actuators dynamics result linear and Laplace Transform can be applied for obtaining the motor model

$$\begin{aligned} \tau_L(s) &= \theta_L(s)(J_L s^2 + b_L s) + z_L(s) \\ \tau_R(s) &= \theta_R(s)(J_R s^2 + b_R s) + z_R(s) \end{aligned} \tag{3}$$

Angular position of the motor/winch sets can be expressed as

$$\begin{aligned} \theta_L(s) &= \frac{1}{J_L s^2 + b_L s} \cdot \tau_L(s) + \frac{1}{J_L s^2 + b_L s} \cdot z_L(s) \\ \theta_R(s) &= \frac{1}{J_R s^2 + b_R s} \cdot \tau_R(s) + \frac{1}{J_R s^2 + b_R s} \cdot z_R(s) \end{aligned} \tag{4}$$

and the transfer function to be controlled can be written as

$$\begin{aligned} G_L(s) &= \frac{\theta_L(s)}{\tau_L(s)} = \frac{A_L}{s(s + B_L)} \\ G_R(s) &= \frac{\theta_R(s)}{\tau_R(s)} = \frac{A_R}{s(s + B_R)} \end{aligned} \tag{5}$$

Assuming a PID controller, $R(s) = K_p + K_d \cdot s + \frac{K_i}{s}$, where K_p, K_i and K_d are the proportional, integral and derivative constant (Ogata 2010), the controllers block shown are

$$\begin{aligned} Controller\ L = R_L(s) &= K_{pL} + K_{dL} \cdot s + \frac{K_{iL}}{s} \\ Controller\ R = R_R(s) &= K_{pR} + K_{dR} \cdot s + \frac{K_{iR}}{s} \end{aligned} \tag{6}$$

Conventional frequency domain tuning method has been applied to obtain the controllers parameters by fixing the desired values of gain crossover frequency and phase margin (Feliu-Batlle and Castillo-García 2014).

5. Simulations

5.1 Preliminaries

Simulations have been developed in Matlab® and Simulink®. A fixed sample time has been set to 1 ms using ode4 (Runge Kutta) as solver. The system has been simulated with the model parameters summarized in Table 1,

Table 1 Model parameters

Subsystem	Parameter	Value	Subsystem	Parameter	Value
Carriage	m_c	1.50 kg	Motor/ winch set	$J_R = J_L$	0.034 kgm^2
	b_c	1.00 Ns/m		$b_R = b_L$	0.039 Nms
	w	0.10 m		r	0.037 m
Frame	W	1.26 m	End-effector	m_e	2.00 kg
	H	2.00 m			

Table 2 Controllers summary

Controller	Gain crossover frequency (rad/s)	Phase margin (°)	K_p	K_i	K_d
L	121	90	4.718	1	4.072
R	121	90	4.718	1	4.072

according to the experimental platform (see Section 6). The controllers parameters, together with the frequency requirements to be obtained are summarized in Table 2.

5.2 Workspace analysis

Static workspace of CDPM can be easily obtained by computing the static equilibrium of force in the end-effector. Let us call τ_{max} the maximum torque that the motor/winch set can exert and T_{min} the minimum tension of cable to avoid saggy effect. The end-effector pose can be located at all the points of the workspace, compute the static equilibrium of force and check if the torque of the motor does not exceed the maximum one, τ_{max} and if the tension is greater than the minimum one, T_{min}. Fig. 8 compares the static workspace of the new proposal to the conventional architecture of CDSM shown in Fig. 3. A maximum allowed torque of 20 Nm and a minimum tension of 5 N have been assumed.

Note that the workspace of the proposal is 16% greater than the conventional architecture of CDPM for the model parameters of Table 1. On the other hand, its boundary box is rectangular allowing to use our proposal for inspection of regular surfaces. For illustrative purpose, Fig. 9 compares both configurations when frame width increments (2 m, 4 m and 6 m). While conventional architecture loses feasible workspace when frame width increases, our proposal increase it and for a 6 m width frame conventional CDSM could only reach 19.80% of the frame since our proposal reaches up to 93.28% of the workspace surface.

5.3 End-effector position control

Dynamics model (1) is a second order system and 4th *Bezier* trajectories has been therefore implemented to ensure smooth trajectories of the end-effector and to avoid abrupt changes in the control signal values which could yield to non-desirable vibration of the end-effector. In order to illustrate the controlled system behavior, a horizontal (Fig. 10) and vertical (Fig. 11) simulations are summarized here.

Fig. 10 shows the result of a horizontal movement from $[x_e^*, y_e^*]_{ini} = [-0.200, 0.150]$ m to $[x_e^*, y_e^*]_{fin} = [0.200, 0.150]$ m. Note that the end-effector pose tracks the reference during all the trajectory. The average error obtained is 0.8 mm and the maximum following error is 1.2 mm.

Fig. 11 represents the result of a vertical movement from $[x_e^*, y_e^*]_{ini} = [0.450, 0.000]$ m to $[x_e^*, y_e^*]_{fin} = [0.150, 0.000]$ m. The end-effector pose tracks again the reference during all the trajectory. The average error obtained is

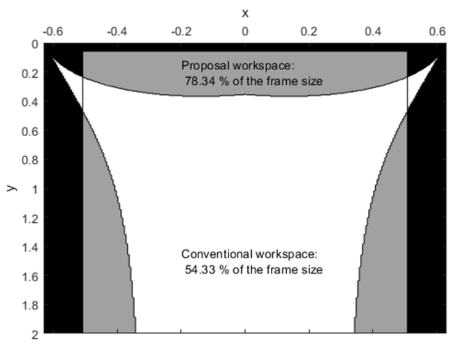

Fig. 8 Workspace comparison: Proposal vs. Conventional CDPM

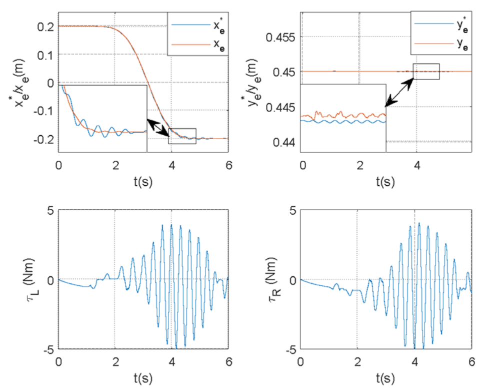

Fig. 10 Simulation: Horizontal movement

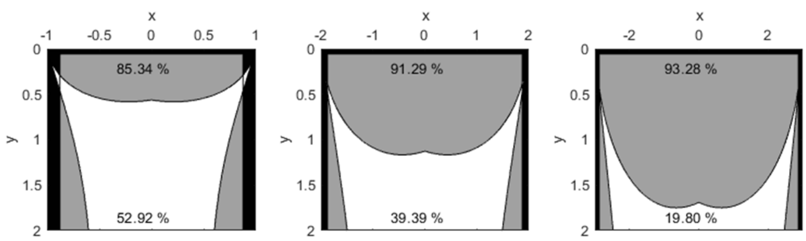

Fig. 9 Workspace comparison when frame width increases

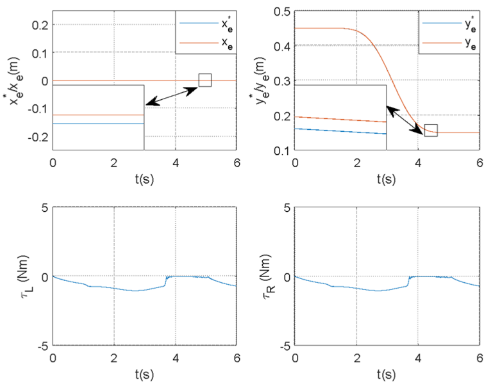

Fig. 11 Simulation: Vertical movement

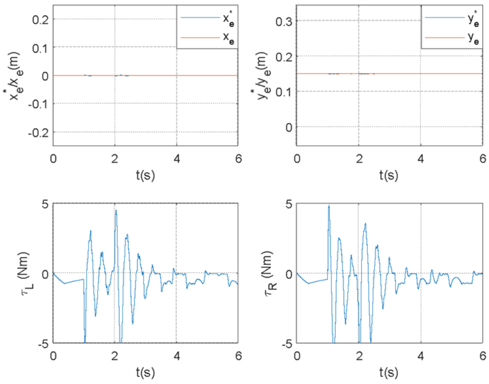

Fig. 12 Simulation: Disturbance rejection

0.4 mm and the maximum following error is 0.8 mm.

Table 3 summarizes the simulations results together to the experimental ones. The obtained error is lower than conventional errors obtained in CDSM which, for this workspace size, is around 10-20 mm (Maloletov *et al.* 2019). Finally, Fig. 12 represents the behavior of the system in presence of a disturbance in the carriage position, modeled as a force pulse of 10 N and a duration of 1 s. Note that the control system can reject the carriage disturbance maintaining the end-effector pose by increasing the control signal, motors torques during the disturbance effect.

6. Experiments

6.1 Platform description

The parameters values of the experimental platform are the same that the ones used in simulations section and summarized in Table 1. The frame is made of *bosch* aluminum profile and the winches and the carriage has been 3D printed in PLA. The motors are DC RE 40 model from *Maxon Motor* that have been couple to a worm gearbox and to the printed winches. Incremental encoders are couple to the motors to measure their angular positions. The carriage position is also measured by means of and incremental encoder by mean of a closed cable loop which rotates a pulley. Two *Maxon Motor* servoamplifier ESCON 70/10 are used for applying the control signal to the motors and a *National Instruments FPGA* based board (*MyRio*) has been used for implementing the real time control. Fig. 13 shows the final aspect of the prototype.

6.2 Results

In order to compute the tracking error of the experiments (in a similar way to simulations), a low-cost vision system has been developed. A 30 fps and 1920 × 1024 resolution camera has been used. Although the resolution of the camera only allows to track the end-effector with a resolution at real world of about 0.25 mm and a sample time of 33 ms.

Fig. 14 illustrates the results of the computer vision tracking algorithm developed in Matlab® for translating image coordinates to world coordinates and track the end-effector pose.

In a similar way to Simulation section, horizontal and vertical movements have been carried out in order to demonstrate the end-effector positioning. For both movements, the same 4th order Bezier trajectories of Simulation section have been implemented for ensuring a smooth evolution of the references and, as consequence, of the control signals.

Figs. 15 and 16 represents the end-effector reference position, x_e^* and y_e^*, the real time estimation of end-

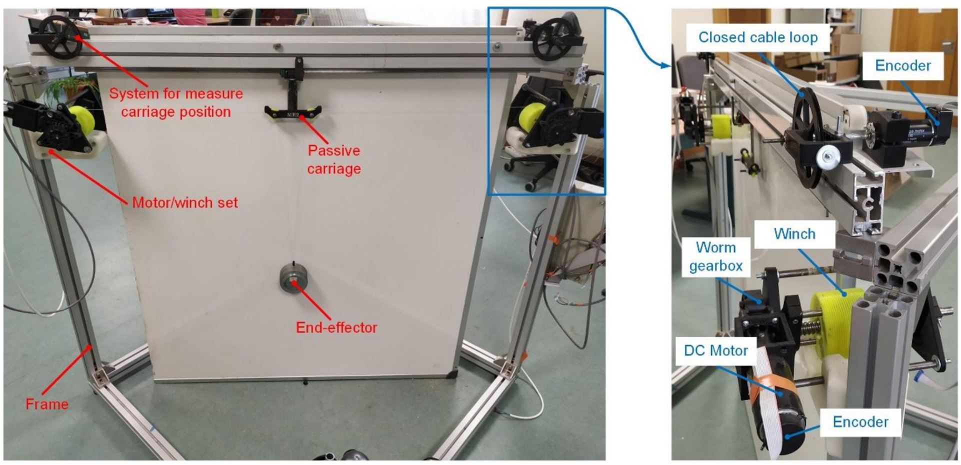

Fig. 13 Experimental platform

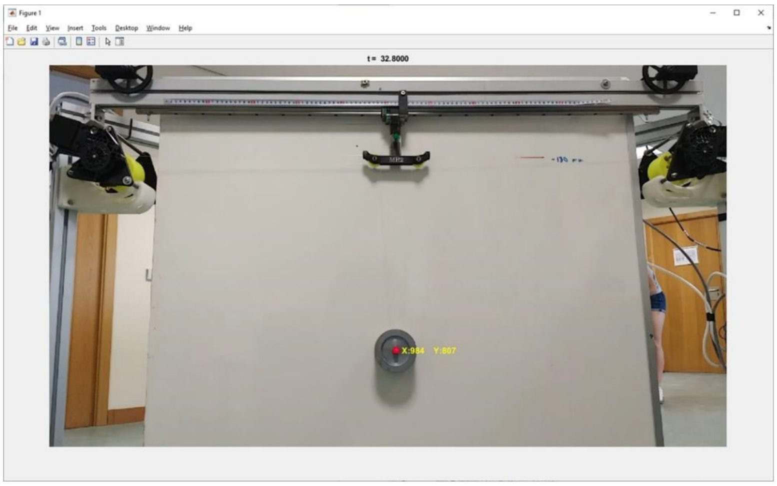

Fig. 14 Vision system for tracking end-effector pose

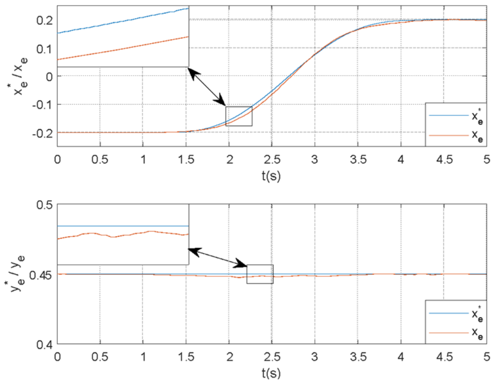

Fig. 15 Experiments: Horizontal movement

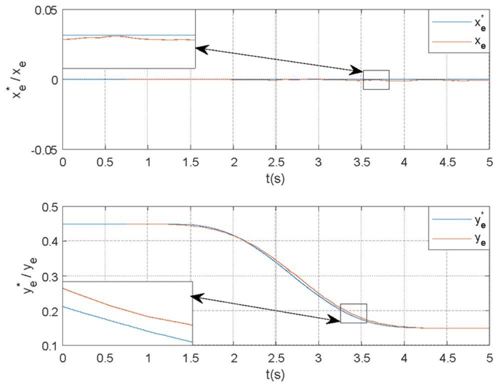

Fig. 16 Experiments: Vertical movement

effector pose, $\hat{x}_e$ and $\hat{y}_e$, and the offline measurement of end-effector pose by means of the vision system, x_e and y_e.

Fig. 15 shows the result of a horizontal movement from $[x_e^*, y_e^*]_{ini} = [-0.200,\ 0.150]$ m to $[x_e^*, y_e^*]_{fin} = [0.200,\ 0.150]$ m. Note that the end-effector pose tracks the reference during all the trajectory. The average error obtained is 3.2 mm and the maximum following error is 16 mm.

Fig. 16 represents the result of a vertical movement from $[x_e^*, y_e^*]_{ini} = [0.450,\ 0.000]$ m to $[x_e^*, y_e^*]_{fin} = [0.150,\ 0.000]$ m. The end-effector pose tracks again the reference during all the trajectory. The average error obtained is 1.7 mm and the maximum following error is 9.4 mm.

Finally, Fig. 17 represents an experiment at which a lateral external force is applied to the carriage. During the Table 3 summarizes the results obtained by simulations and experiments.

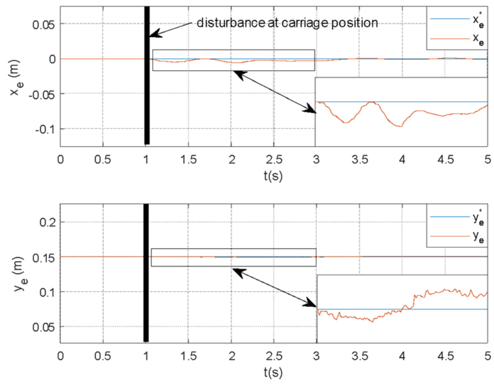

Fig. 17 Experiments: Disturbance rejection

Table 3 Summary of simulations and experiments

Movement	Initial pose (m)	Final pose (m)	Trajectory time (s)	Simulation /Experiments	Average following error (mm)	Maximum following error (mm)
Horizontal	[-0.20,0.15]	[0.20,0.15]	4	Simulation	0.8	1.2
				Experiment	3.2	16
Vertical	[0.45,0.00]	[0.15,0.00]	4	Simulation	0.4	0.8
				Experiment	1.7	9.4

application of the force (about 20 N) the controller is able to maintain the end-effector pose at the reference pose $[x_e^*, y_e^*] = [0, 0.15]$ m. The maximum divergence of the end-effector pose during the experiment is about 2 mm. These lateral external forces are intended to simulate real forces that the robot can suffer when operating in the presence of strong winds (Jeong *et al*. 2019).

7. Conclusions

In this work, a novel mechanical design based in the addition of a passive carriage to the upper part of the frame in a 2 degrees-of-freedom cable suspended robot has been proposed. The aim of this design is to significantly enlarge the robot workspace without increasing the torque requirements of the motors, allowing its application to the automatic inspection of large surfaces as the ones in civil infrastructures due to an efficient control system. A specific control approach has been designed for the elimination of vibrations that appeared inherent to the new design and also cancelling the effect of perturbations. For the validation of the mechanical and control proposals, both the robot dynamics and the control system have been mathematically modeled. Several tracking trajectories for the end-effector have been simulated, obtaining a tracking error not higher than 1mm and a good robustness to lateral force perturbations, similar to the ones that the robot can suffer in real operation conditions. To validate these results, a prototype with the same parameters has been built, the control system has been implemented in a real-time hardware and the simulations have been replicated experimentally, obtaining a very low tracking error and also observing a good capacity to reject force perturbations and maintaining the end-effector pose.

Further works in this research line must include the attaching of different inspection systems to the end-effector as cameras or laser to detect, reconstruct and analyze different kind of defects present in vertical surfaces of civil infrastructures as facades, dams or even in other fields as marine or aerospace engineering to inspect large ships or aircrafts, thanks to the modularity and quick deployment capacity of suspended cable robots.

Acknowledgments

The research described in this paper was financially supported by Research Fund for Coal and Steel grant agreement No. 800687 in the framework of DESDEMONA project. Authors wish to thank the financial Support provided by the university of Castilla-La Mancha and the European Social Fund through the pre-doctoral funding [2019/451].

References

Abbasnejad, G. and Carricato, M. (2012), "Real solutions of the direct geometrico-static problem of under-constrained cable-driven parallel robots with 3 cables: A numerical investigation", *Meccanica*, **47**(7), 1761-1773. https://doi.org/10.1007/s11012-012-9552-3

Adhikari, R.S., Bagchi, A. and Moselhi, O. (2014), "Automated condition assessment of concrete bridges with digital imaging", *Smart Struct. Syst., Int. J.*, **13**(6), 901-925. https://doi.org/10.12989/SSS.2014.13.6.901

Arsenault, M. (2013), "Stiffness analysis of a planar 2-dof cable-suspended mechanism while considering cable mass", In: *Cable-Driven Parallel Robots* (pp. 405-421), Springer, Berlin, Heidelberg.

Behzadipour, S. (2006), "Stiffness of cable-based parallel manipulators with application to stability analysis", *J. Mech. Des.*, **128**(1), 303-310.

BostelMan, R., Albus, J., Dagalakis, N. and Jacoff, A. (1996), "Robocrane project: an advanced concept for large scale manufacturing", In: *AUVSI-PROCEEDINGS-*, Citeseer, pp. 509-522.

CableRobot Simulator (2020), "Cable-driven parallel robots – motion simulation in a new dimension", Accessed: 2020-07-02. http://www.ipa.fraunhofer.de/en/cable-driven_parallel_robots.html

Castelli, G., Ottaviano, E. and González, A. (2010), "Analysis and simulation of a new Cartesian cable-suspended robot", *Proceedings of the Institution of Mechanical Engineers, Part C: Journal of Mechanical Engineering Science*, **224**(8), 1717-1726.

Castelli, G., Ottaviano, E. and Rea, P. (2014), "A Cartesian cable-suspended robot for improving end-users mobility in an urban environment", *Robot. Comput.-Integr. Manuf.*, **30**(3), 335-343.

Castillo-Garcia, F.J., Rea, P., Gonzalez-Rodriguez, A. and Ottaviano, E. (2017), "On the Design of a 4 Degrees-of-freedom Pick and Place Cable Suspended Parallel Manipulator", *Int. J. Robot. Automat.* (*IJRA*), **6**(4), 286-302.

CoGiRo Project (2020), Accessed: 2020-07-10. http://www.lirmm.fr/cogiro/

Cone, L.L. (1985), "Skycam-an aerial robotic camera system", *Byte*, **10**(10), 122.

Fattah, A. and Agrawal, S.K. (2002), "Workspace and design analysis of cable-suspended planar parallel robots", *Proceedings of International Design Engineering Technical Conferences and Computers and Information in Engineering Conference*, Vol. 36533, pp. 1095-1103.

Feliu-Batlle, V. and Castillo-García, F.J. (2014), "On the robust control of stable minimum phase plants with large uncertainty in a time constant, A fractional-order control approach", *Automatica*, **50**(1), 218-224.

Gonzalez-Rodriguez, A., Castillo-Garcia, F.J., Ottaviano, E., Rea, P. and Gonzalez-Rodriguez, A.G. (2017), "On the effects of the design of cable-Driven robots on kinematics and dynamics models accuracy", *Mechatronics*, **43**, 18-27. http://dx.doi.org/10.1016/j.mechatronics.2017.02.002

Gouttefarde, M. (2008), "Characterizations of fully constrained poses of parallel cable-driven robots: a review", *Proceedings of International Design Engineering Technical Conferences and Computers and Information in Engineering Conference*, Vol. 43260, pp. 21-30.

Huang, T.L., Zhou, H., Chen, H.P. and Ren, W.X. (2016), "Stochastic modelling and optimum inspection and maintenance strategy for fatigue affected steel bridge members", *Smart Struct. Syst., Int. J.*, **18**(3), 569-584. https://doi.org/10.12989/SSS.2016.18.3.569

Jeong, S., Lee, J., Cho, S. and Sim, S.H. (2019), "Integrated cable vibration control system using Arduino", *Smart Struct. Syst., Int. J.*, **23**(6), 695-702. https://doi.org/10.12989/sss.2019.23.6.695

Jung, H.-J., Lee, J.-H., Yoon, S. and Kim, I.-H. (2019), "Bridge Inspection and condition assessment using Unmanned Aerial Vehicles (UAVs): Major challenges and solutions from a

practical perspective", *Smart Struct. Syst., Int. J.*, **24**(5), 669-681. https://doi.org/10.12989/SSS.2019.24.5.669
Kawamura, S., Choe, W., Tanaka, S. and Pandian, S.R. (1995), "Development of an ultrahigh speed robot falcon using wire drive system", In: *Proceedings of IEEE International Conference on Robotics and Automation*, **1**, 215-220.
Kawamura, S., Kino, H. and Won, C. (2000), "High-speed manipulation by using parallel wiredriven robots", *Robotica*, **18**(1), 13-21.
Kim, C.W., Isemoto, R., McGetrick, P.J., Kawatani, M. and OBrien, E.J. (2014), "Drive-by bridge inspection from three different approaches", *Smart Struct. Syst., Int. J.*, **13**(5), 775-796. https://doi.org/10.12989/SSS.2014.13.5.775
Lee, A.Y., Oh, J.K. and Choi, Y.J. (2010), "Bridge Inspection System using Robot", *J. Korea Robot. Soc.*, **5**(1), 77-84.
Maloletov, A.V., Fadeev, M.Y. and Klimchik, A.S. (2019), "Error Analysis in Solving the Inverse Problem of the Cable-driven Parallel Underactuated Robot Kinematics and Methods for their Elimination", *IFAC-PapersOnLine*, **52**(13), 1156-1161.
Merlet, J.-P. and dit Sandretto, J.A. (2015), "The forward kinematics of cable-driven parallel robots with sagging cables", In: Book; *Cable-Driven 190 Parallel Robots Editors: Andreas Pott, Tobias Bruckmann. Proceedings of the Second International Conference on Cable-Driven Parallel Robots, Book Series: Mechanisms and Machine Science*, **32**, 3-15.
Nan, R. (2006), "Five hundred meter aperture spherical radio telescope (fast)", *Sci. China Series G*, **49**(2), 129-148.
Ogata, K. (2010), *Modern Control Engineering*, Prentice hall
Ottaviano, E. and Castelli, G. (2010), "A Study on the Effects of Cable Mass and Elasticity in Cable-Based Parallel Manipulators", *Proceedings of the 18th CISM-IFToMM Symposium on Robot Design, Dynamics and Control*, Springer Ed. Udine, pp. 149-156.
Ottaviano, E., Arena, A., Gattulli, V. and Potenza, F. (2019), "Slackening effects in 2D exact positioning in cable-driven parallel manipulators", In: A. Pott, T. Bruckmann (Eds.), *Mechanisms and Machine Science, Vol. 74 of Cable-Driven Parallel Robots. CableCon 2019*, Springer, Cham, pp. 319-330.
Pott, A. (2018a), "Kinematic Codes", In: *Cable-Driven Parallel Robots*, Springer Tracts in Advanced Robotics, Vol. 120, Springer, Cham.
Pott, A. (2018b), "Kinematics with Nonstandard Cable Models", In: *Cable-Driven Parallel Robots*, Springer Tracts in Advanced Robotics, Vol. 120, Springer, Cham.
Pott, A., Mutherich, H., Kraus, W., Schmidt, V., Miermeister, P., Dietz, T. and Verl, A. (2013), "Cable-driven parallel robots for industrial applications: The ipanema system family", *Proceedings of the 44th International Symposium on Robotics* (*ISR*), pp. 1-6.
Pusey, J., Fattah, A., Agrawal, S. and Messina, E. (2004), "Design and workspace analysis of a 6–6 cable-suspended parallel robot", *Mech. Mach. Theory*, **39**(7), 761-778.
Roberts, R., Graham, T. and Lippitt, T. (1998), "On the inverse kinematics, statics, and fault tolerance of cable-suspended robots", *J. Robot. Syst.*, **15**(10), 581-597.
Rubio-Gómez, G., Rodríguez-Rosa, D., García-Vanegas, J.A., Gonzalez-Rodríguez, A., Castillo-García, F.J. and Ottaviano, E. (2019), "Chain Driven Robots: An Industrial Application Opportunity. A Planar Case Approach", In: *International Conference on Cable-Driven Parallel Robots*, Springer, Cham, pp. 13-22.
Skycam (2020), Accessed: 2020-07-10. https://en.wikipedia.org/wiki/Skycam
Wang, Q., Kim, M.K., Sohn, H. and Cheng, J.C. (2016), "Surface flatness and distortion inspection of precast concrete elements using laser scanning technology", *Smart Struct. Syst., Int. J.*, **18**(3), 601-623. https://doi.org/10.12989/sss.2016.18.3.601
Yangwen, X., Qi, L., Yaqing, Z. and Bin, L. (2010), "Model aerodynamic tests with a wire-driven parallel suspension system in low-speed wind tunnel", *Chinese J. Aeronaut.*, **23**(4), 393-400. https://doi.org/10.1016/S1000-9361(09)60233-8

Appendix A. Kinematics problem expression

Assuming an initial position for the end effector (x_{e0}, y_{e0}), the initial cable length can be computed as

$$\begin{aligned} L_{10} &= \frac{D}{2} - x_{e0} - \frac{w}{2} \\ L_{20} &= \left(\left(\frac{d}{2}\right)^2 + y_{e0}^2\right)^{\frac{1}{2}} \\ L_{30} &= L_{20} \\ L_{40} &= D - w - L_{10} \end{aligned} \tag{A1}$$

Assuming $x_c = x_e$, the cable lengths for any position of the end-effector can be calculated as

$$\begin{aligned} L_1 &= \frac{D}{2} - x_c - \frac{w}{2} \\ L_{40} &= D - w - L_1 \\ L_3 &= \left(y_e^2 + \left(x_e - L_4 + \frac{D}{2}\right)^2\right)^{\frac{1}{2}} \\ L_2 &= \left(y_e^2 + \left(-x_e - L_1 + \frac{D}{2}\right)^2\right)^{1/2} \end{aligned} \tag{A2}$$

And the inverse kinematics model yields

$$\begin{aligned} [\theta_L\ \theta_R\ ] &= \Lambda^I(x_e, y_e, x_c) \\ &= \frac{1}{r} \cdot [L_1 + L_2 - L_{10} - L_{20}\ L_3 + L_4 - L_{30} - L_{40}\ ] \end{aligned} \tag{A3}$$

On the other hand, considering that both the motor angles and the carriage position is known, the lengths of the cables can be computed as

$$\begin{aligned} L_1 &= \frac{D}{2} - x_c - \frac{w}{2} \\ L_4 &= \frac{D}{2} + x_c - \frac{w}{2} \\ L_2 &= r\theta_L + L_{10} + L_{20} - L_1 \\ L_3 &= r\theta_R + L_{30} + L_{40} - L_4 \end{aligned} \tag{A4}$$

Finally, the estimator block, $[\hat{x}_e, \hat{y}_e] = \Xi(x_c,\ \theta_L, \theta_R)$ yields as

$$\begin{aligned} [x_e\ y_e\ ] &= \Xi(x_c, \theta_L, \theta_R) \\ &= \left[\frac{L_3^2 + 2wx_c - L_2^2}{2w}\ \frac{a \cdot b \cdot c \cdot e}{2w}\right] \end{aligned} \tag{A5}$$

being $a = L_2 + L_3 + w$, $b = (L_2 + L_3 - d)$, $c = L_2 - L_3 + d$ and $e = L_3 - L_2 + d$.